Integrated object tracking framework for range gated camera systems

Mustafa Yağcıoğlu [a] , Kuthan Yelen [a] , Alptekin Temizel [b]

[a]ASELSAN A.Ş., Aselsan MGEO, Ankara-TURKEY

[b]Middle East Technical University, Informatics Institute, Ankara-TURKEY

ABSTRACT

Range-gated imaging systems are active systems which use a high-power pulsed-light source and control the opening and closing times of the camera shutter in conjunction with the light source. By calculating the arrival time of the reflected light from the object, the camera shutter is opened for a short time period to form an image using the returned light. This allows generating high contrast images of the objects in difficult lighting conditions. On the other hand the object distance needs to be known and operators are expected to select the proper shutter timing to keep the object of interest continuously in the view. In order to automate this procedure, a tracking system needs to provide feedback to adjust camera shutter timing by estimating the distance of the object in addition to its horizontal and vertical position. In this paper, we present an object tracking framework integrated to the range-gated camera setup without resorting to an additional laser or radar based range finder unit even the object distance changes during the tracking. Range estimation is solely based on image processing and the distance of the object is estimated by the proposed algorithm with a number of similarity measurement methods. The performances of these methods are compared for various scenarios using the data acquired by the range-gated system setup.

Keywords: Range gated cameras, object tracking, night vision systems

1. INTRODUCTION

Video surveillance systems predominantly use visible-light, near infrared or thermal sensors for object tracking. Visible-light camera systems require illumination and suffer from low light conditions. Similar to visible-band cameras, near-infrared cameras also require active illumination in the respective spectrum, limiting their range of operation. On the other hand, while thermal cameras do not require any illumination, they cannot provide texture or reflectance information of the object and the object should dissipate heat to be visible in thermal images. Range gated imaging systems have the capability of getting images from long distances and from any object at the absence of light in the environment. These systems consist of a laser emitter and a camera with adjustable gate. Illumination of the scene is achieved by the laser pulse and the camera gate is synchronized with the return of the laser pulse from the scene. These systems have the following advantages compared to the conventional imaging systems:

- Use of laser light for illumination allows imaging at a long range,

- By only opening the gate briefly to allow only desired light to reach to the sensors, the system attains a high signal to noise ratio,

- Contrary to thermal imaging systems, the objects are not expected to dissipate heat and the images have texture and reflectance information.

Range gated camera systems have been actively researched in order to achieve better performance in night vision applications. Since such systems require multidisciplinary work and applications are mainly in the military domain, there is limited amount of published work on this subject and most of the articles on range gated camera systems focus on the system construction. Two prominent application areas of these systems are 3D scene construction and 2D imaging at low light conditions.

1.1 Range Gated Imaging Studies

History of the range gated camera system begins with the development of the first concepts in the 1960s. Neuman[1] was granted the first patent in 1968 by the United States Patent Office. He proposed a system with Q-switched 60 nanoseconds gated laser pulse and 50 nanoseconds camera gate. Kerpchar[2] proposed an underwater range gated imaging system in 1972. The system is worn by a diver and the gate and delay times of the system are configurable by the diver. At 1990, Ulich et al.[3] were granted a patent for using multiple cameras which are independently configurable with

different delay and gating times. They claimed that by using such a system, sub-images of a scene can be obtained by only one light pulse. One year later, Ulich et al.[4] were granted a patent for an imaging camera which includes pulsed light source, camera and timing electronics internally.

Most published work on range gated camera systems focus on the system description. Bonnier and Larochelle[5] describe the properties of their range gated system that they named airborne laser based enhanced detection and observation system (ALBEDOS) for coast guard and maritime. ALBEDOS is based on a powerful laser diode array illuminator and a range-gated low-light-level TV camera. Repasi et al.[6] locate laser and the camera at different locations (in classical approach, laser source and camera are located at the same location) and acquire images. They also aim to acquire images even when the object is not in the line of sight of the camera by using the walls as mirrors. By this method, they can get the image of a person who is standing 20 meters away from the illuminated wall. Fect and Rothe[7] discuss the development and compare the experimental results of two imaging laser radar systems based on range gating. One of the systems operates with 1574 nm eye safe laser and the other operates with 532nm laser. Ofer et al.[8] developed an active night vision system using gated imaging principles. There are also a number of underwater applications. Weiqi et al.[9] describe an underwater imaging system and claim that they reach 30 meter visibility at turbid medium. Tan et al.[10] also work on the turbid water medium and compare the images obtained from different turbidity levels. The U.S. Army and the U.S. Air Force are aggressively pursuing programs that utilize laser range-gated, shortwave IR imaging systems to perform long range target identification. Driggers et al.[11] investigated the impact of speckle on laser range-gated shortwave infrared imaging system on target identification performance.

Determining the properties of the system is a challenging task. Power of the laser unit, gating time of the laser pulse and the camera unit and performance of the intensifier are the main parameters which need to be determined. Zhang et al.[12] give detailed information for the properties of the system.

Improvement of the quality of the obtained range-gated images is another field of study. Gilles[13] proposes some image processing algorithms to eliminate the artifacts on range gated images. He compares the effects of applying mean and median filters and evaluated the results. Repasi et. al.[14] propose taking the average of images to reduce the speckle. An approach to modeling the performance of active imaging systems has been introduced by Richard et.al[15]. This approach leverages physically accurate models of speckle, scintillation, and psychophysically accurate models of target acquisition.

Another line of work utilizing range gated camera systems is on 3D reconstruction. Busck and Heiselberg[16] proposed a method for 3D object reconstruction by using the images taken from a gated system. They obtained better than 1 mm range accuracy by using 200 picoseconds gate time. Laurenzis[17] claims that the whole depth information can be calculated from a minimum number of two range-gated images via the super-resolution depth mapping technique. Laurenzis and Bacher[18] discuss a method of image coding by multiple exposure of range gated images. Their claim is that they can enlarge the depth mapping range by a factor of 12 by using three range gated images. Following this work, Laurenzis et al.[19] proposed an improved algorithm that uses quasi-ambiguous coding sequences to enlarge the depth mapping by a factor of 13. Anderson[20] suggests two different methods and investigates algorithm performance through Monte Carlo simulations using a simplified system and imaging model. Monnin et al.[21] state that by precisely synchronizing both the illuminator and the camera shutter, it is possible to acquire "slices" of the scene at specific known distances. They show that even with large laser pulses and without megahertz-capable electronics, the third dimension can be recovered for the whole range of the scene by processing only two images acquired in specific conditions. Steinvall et al.[22] provided a review of various work on range gated imaging undertaken at the Swedish Defence Research Agency (FOI). The basis for 3-D scene reconstruction is an image sequence acquired using a sliding gate delay time. Göhler and Lutzmann[23] investigated the influence of the number of averaged images on the resulting range accuracy. They located a well-defined plate as an object and used brightness of each pixel of the plate to calculate the range error for different number of averaged images.

1.2 Object Trackers

While there is a great deal of interest in object tracking algorithms using visible-band and thermal images (Yilmaz et al.[24] provided an extensive survey on object tracking), object tracking with range gated camera systems is a fairly unexplored research field because of the lack of common availability of range gated systems.

Most of the object tracking methods are based on the 2D intensity images. Kristan et al.[25] developed a tracker that combines optical flow and color based particle filter. Kodama et al.[26] proposed a technique for tracking the velocity of objects that combines the particle filter with optical flow. Tung and Matsuyama[27] proposed a solution to human motion

tracking by using a color-based particle filter driven by optical flow. Beyan and Temizel[28] proposed a surveillance system for indoor environments which is capable of tracking multiple objects using both visible and thermal band images. Beyan and Temizel[33] also used adaptive background modeling in association with mean-shift tracking for fully automatic tracking.

Spies et al.[29] discussed the computation of the instantaneous 3D displacement vector fields of deformable surfaces from sequences of range data. Barron and Spies[30] combined the 2D optical flow method and 3D range flow methods to achieve better tracking performance.

Tracking algorithms require an object detection mechanism for initialization. Besides using the information on a single frame, temporal information can also be used for object detection. Background subtraction is a popular method using temporal information. Background of the scene is modeled and the difference of the new images and the background model is detected as object. Wren et al.[31] proposed a human tracker system that they called Pfinder (person finder). Since the camera is fixed, Pfinder models the background scene that is relatively static. Then, when a human enters the scene it begins to build up a model of that person. Beyan and Temizel[32] present a fully automatic multiple-object tracker based on mean-shift algorithm. They detect new objects entering to the field of view and objects that are leaving the scene by using foreground detection.

Although there are a number of studies on range gated imaging systems, most of the studies focus on the system construction, 3D reconstruction and enhancement of images obtained by range gated systems. Automated object tracking on such a system is desirable as it would eliminate the need for a human operator to continuously set the gate timing for the changing object distance and allow the object to remain in sight all the time without any user intervention. However, there is no object tracking work specifically designed for a range gated system to our knowledge.

2. METHODOLOGY

In this article, an active object tracking algorithm working in association with the range gated camera system is described. The distance of the object estimated by the tracking algorithm is used by the range gated system to obtain the subsequent image without resorting to an additional laser or radar based range finder unit. Range estimation is solely based on image processing. Components of the active tracking system are shown in Figure 1.
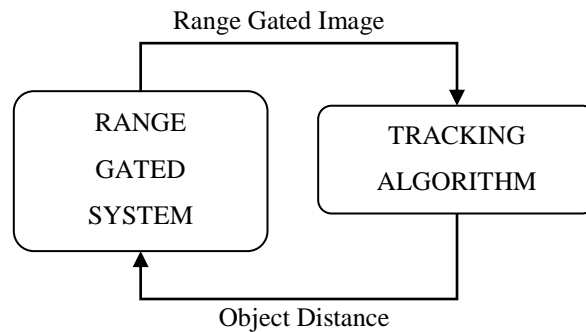

Figure 1 Active tracking system components.

2.1 Working principle

In a range gated imaging system, a camera with tightly controlled opening and closing shutter times is used in conjunction with a high power pulsed light source. Exposure time of the camera and the light source pulse width are arranged according to the return time of the emitted light pulse. Working principle of the gated imaging system is shown at Figure 2.
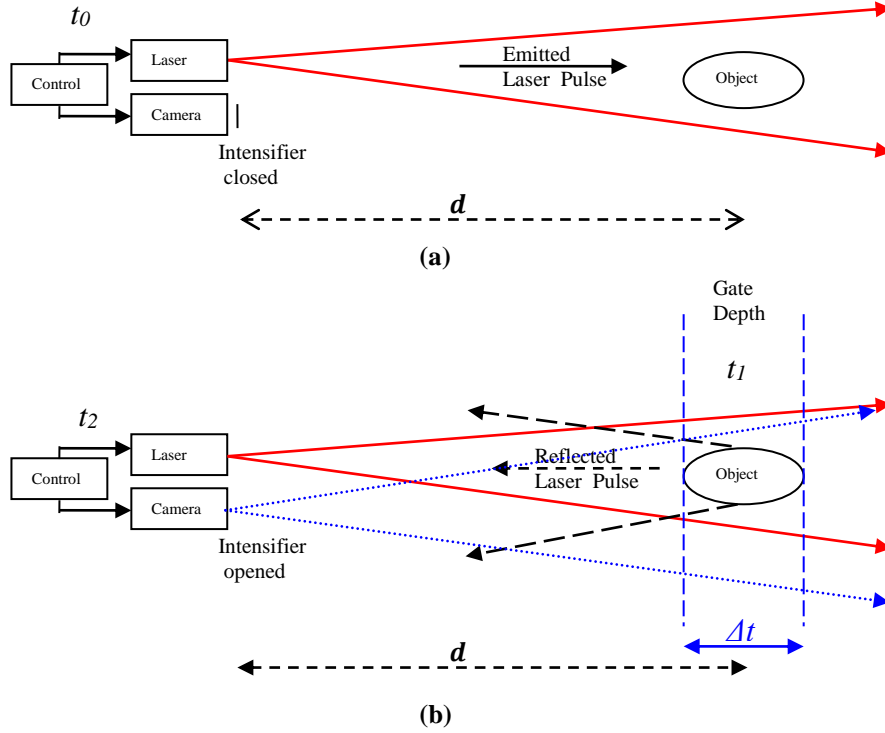
Figure 2 Working principle of range gated systems. (a) Laser pulse is emitted; camera shutter is closed, (b) Emitted laser is reflected, shutter is opened for a short time period.

Steps of the Figure 2 can be summarized as:

- A laser pulse is emitted at t_0 while camera shutter is closed.

- At t_1, emitted light pulse is reflected from the targeted object that is located at distance d.

- At t_2, the camera is opened for a short period (Δt) corresponding to the desired depth of view.

    Return time r that is defined as $t_2 - t_0$, is calculated as;

$$r = \frac{(2 \times d)}{c}$$

(1)

where c is the speed of the light and d is the distance of the object. It is the duration that the emitted light reaches the object and returns to the camera. Controller sets the opening time of the intensifier by using this r value. 'Depth of view' is the depth of the desired illumination area. It is used for the calculation of the 'gate time' of the camera.

2.2 Gated Imaging

Range gated imaging is based on the synchronization of the reflected laser pulse and the sensor gate time. Since only the reflected pulses from the objects that reach the camera at the gating time contributes to the image, the image includes both reflectance and the depth information.

As shown in Figure 3, relative timings of the sensor gate and the laser pulse determine the imaged distance. The emitted laser pulse illuminates the related area in positive z direction. At the same time, sensor gate collects the laser pulses reflected from the objects at the positive z direction at only during the sensor gate time. The convolution of the laser pulse and the sensor gate contributes to the image.
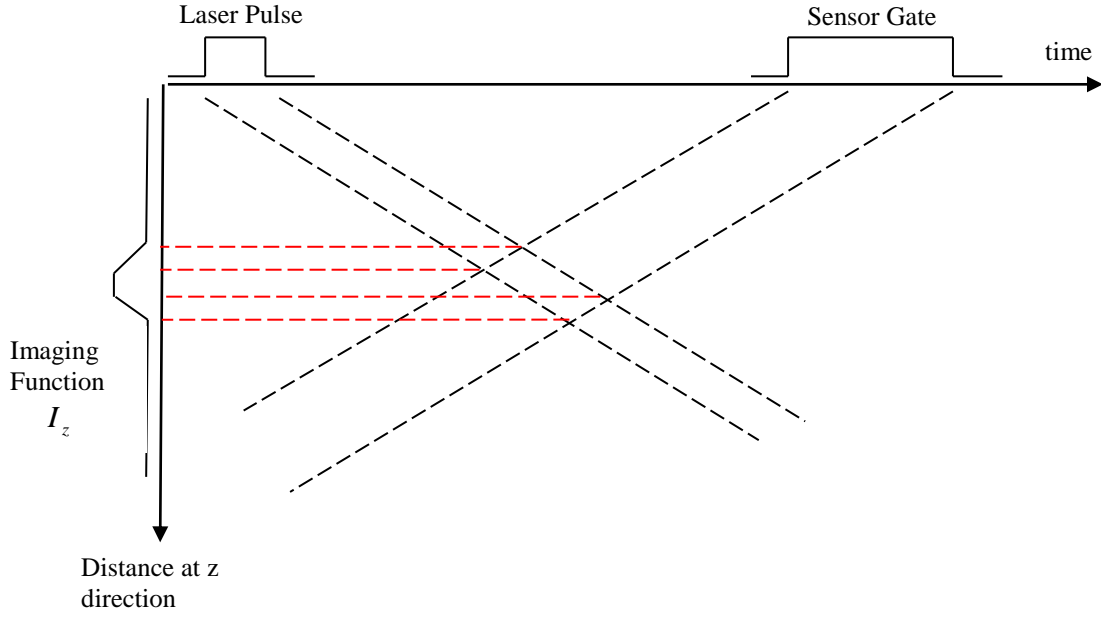
Figure 3 Distance-time model for gated viewing

As illustrated in Figure 3, depth-intensity profile can be calculated from the sensor gate and the laser pulse by taking the convolution of two functions. Effects of the gate delay time and round trip time of the laser must be included in the convolution operation.

$$I_z = \oint_{-\infty}^{\infty} P(t - t_l)G(t - t_s)dt \tag{2}$$

where t_l is the round trip time of the laser pulse, P is the pulse function, t_s is the delay time for the sensor gate and G is the gating function. By arranging the laser pulse, sensor gate and the delay time of the sensor, we can observe different I_z function - image pairs.

2.3   Algorithm Description

In this section, details of the proposed algorithm for object tracking in a range gated system are provided. X-Y Tracking Module tracks the object at every frame. After each successful tracking, reference object image is updated. If the tracking fails or a predefined time passes, Z Tracking Module intervenes to update the object distance. Figure 4 summarizes the whole algorithm and the following sections describe the details of the algorithm.
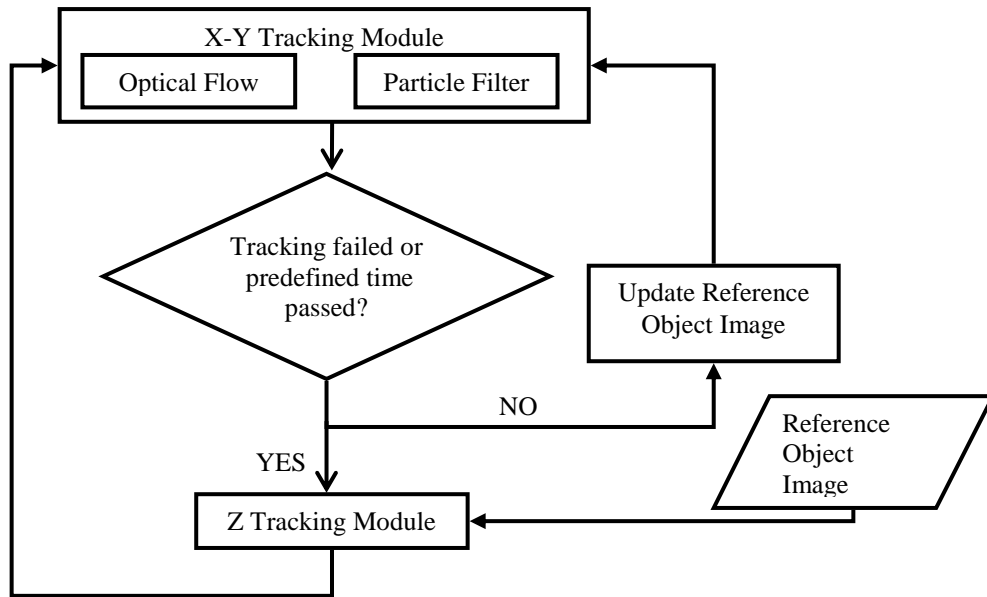
Figure 4 Summary of the proposed object tracking framework.

2.3.1 X-Y Tracking Module

Particle filter method without using the velocity information in transition model gives satisfactory results if the object is stationary or has small movement between consecutive frames. However, sudden movements of the objects results in failure if the Gaussian window around the current state is used as the transition model. Using the velocity and acceleration information also has drawbacks in sudden movement of the object. In order to get satisfactory results, we need to estimate the movement of the related object. Kodama et al.[26] propose a technique for tracking the objects by combining particle filter and optical flow. Pyramidal Lucas Kanade Optical Flow algorithm is implemented by using the features found by Shi and Tomasi feature detector. Optical flow is used in the state transition step of the particle filter technique. In this study, we adopted this technique for tracking in X-Y directions.

Different to the RGB images, range gated images are grayscale images and have higher noise characteristics, which need additional investigation for the usage of optical flow and particle filter. As shown in Figure 5, due to the nature of the range gated images, only a limited distance is illuminated. This results in many dark pixels around the object, adversely affecting the optical flow algorithm. As it is seen in Figure 5, optical flow method generates many motion vectors. To alleviate the effect of these incorrect matches in range gated image, we used an outlier removal step after optical flow. Firstly, the magnitudes of motion vectors are analyzed to remove the outliers. Then, the outlier points in the second image are removed. The motion vector representing the crude motion of the object is obtained by averaging the motion vectors of the remaining features.
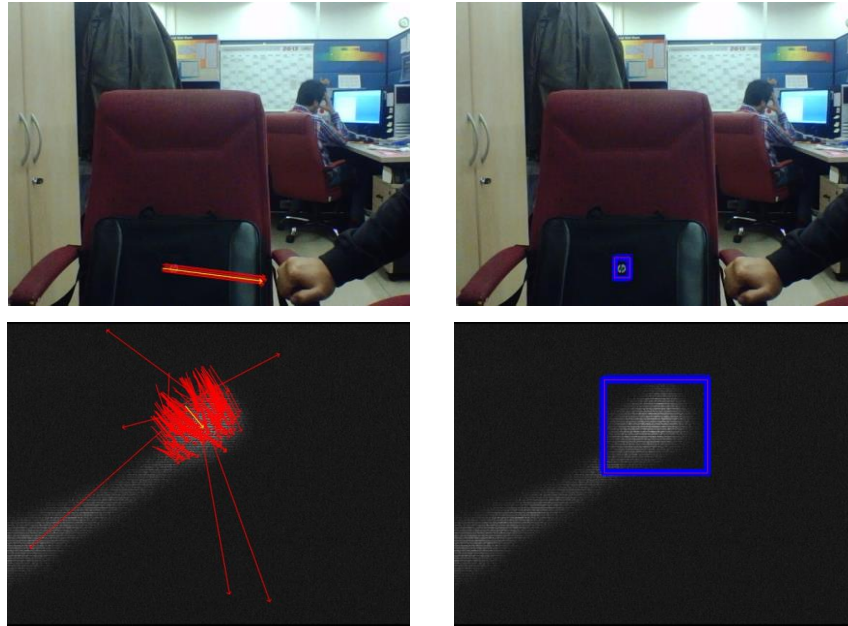
Figure 5 Optical flow output (left) and particle filter output with optical flow feedback (right) for RGB image and Range Gated Image

2.3.2   Z-Tracking Module

Since the moving object is illuminated by using the distance information between the object and the system, incorrect distance information results in the loss of the tracked object in the acquired image. Object distance d must be estimated in real time in order to continue to get new range-gated images at the estimated distance. The proposed Z-tracking module generates this critical information to feed into the range gated camera system.

Getting images from only a single gate depth (Δt) is not sufficient to estimate the distance changes as the object might move towards, or away from the camera. To track the object continuously, the proposed system acquires a number of images nearer from and further away of the last known position of the tracked object as shown in Figure 6.
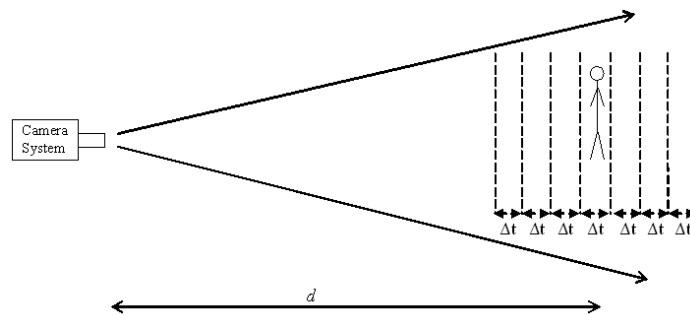
Figure 6 Image slices around the tracked object.

The images taken nearer than and further away of the object are used to calculate the new estimated location of the object. By updating the distance d at each cycle, system keeps the object in the illuminated depth range even it moves towards, or away from the camera. Then the X-Y tracker tracks the object in X and Y directions. Figure 7 illustrates the proposed object tracking algorithm for two iterations.
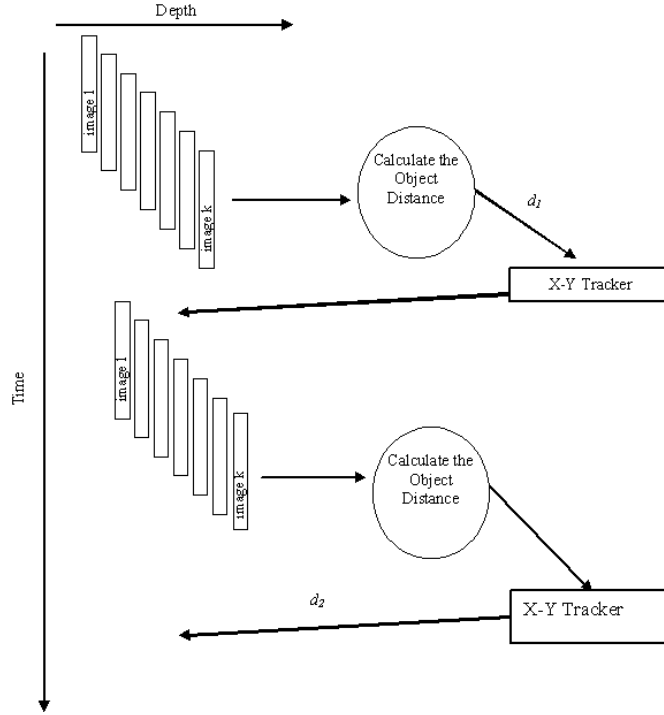
Figure 7 Summary of Object Tracking Algorithm

The object region calculated from X-Y Tracker is given as input to the Z-Tracker. Images are analyzed with Histogram Comparison, Pixel-wise Comparison, Image Brightness, Mutual Information, Peak Signal to Noise Ratio, and Structural Similarity point of views to determine the exact location of the object robustly.

2.3.2.1 Histogram Comparison (HC)

Histogram of each candidate image is compared with that of the reference image to calculate a similarity value. Histogram Likelihood (HL) of two images is calculated by summing up the intersection of two histograms. Each image is scored proportional to its likelihood with the reference image. Eq. 3 gives the calculation method for histogram likelihood.

$$HL = \sum_{k=0}^{K} min\left(H_{ref(k)}, H_{cand(k)}\right) \tag{3}$$

where H_{ref} is the histogram of the reference image, H_{cand} is the histogram of the candidate image, and K is the size of the histogram.

2.3.2.2 Pixel-wise Comparison (PwC)

Similarity between the current image and the reference image gives information about the object distance. The delay time determines the target distance and if it set to a value to obtain images closer to the actual object location, similarity will be higher. Prior to the pixel-wise comparison, image is convolved with a Gaussian kernel to increase robustness to translation and image noise. Eq. 4 gives the equation for calculating the likelihood between two images. Image Likelihood (IL) is used as an indicator of the similarity between two images.

$$DIFF = \sum_{x=0}^{M} \sum_{y=0}^{N} I_1(x,y) - I_2(x,y)$$

$$IL = \frac{1}{DIFF} \tag{4}$$

where I_1 and I_2 are the two images, M and N are the row and column number of the images.

2.3.2.3 Image Brightness (IB)

Image Brightness (IB) is a good indicator of the distance of the object. If the object is on the screen and the used delay time is correct it is expected to appear bright. If the delay time is not correct, images will be obtained from further away or nearer than the object and will have less brightness.

Image Brightness (IB) is a good indicator of the distance of the object. If image brightness is high, the object is on the screen and the used delay is correct. If not, the distance of the object is not determined correctly.

$$IB(I) = \sum_{x=0}^{M} \sum_{y=0}^{N} I(x, y) \tag{5}$$

where I is the image, M and N are the height and width of the image respectively.

2.3.2.4 Mutual Information (MI)

Mutual information has emerged as a similarity measure in the recent years, e.g. Russakoff et al. [34] who used Mutual Information for measuring the similarity between image regions. Mutual information of two images I_1 and I_2 is calculated by using both joint entropy $H(I_1, I_2)$ and the individual entropies $H(I_1)$ and $H(I_2)$.

$$H(I_1, I_2) = -\sum_{a,b} p_{I_1 I_2}(i_1, i_2) \log p_{I_1 I_2}(i_1, i_2), \tag{6}$$

$$H(I_1) = -\sum_{a} p_{I_1}(i_1) \log p_{I_1}(i_1), \tag{7}$$

where $p_{I_1 I_2}$ is the joint probability distribution of pixels associated with images I_1 and I_2. By using the joint entropy and individual entropies defined in equations (6) and (7), mutual information is defined as:

$$MI(I_1, I_2) = H(I_1) + H(I_2) - H(I_1, I_2). \tag{8}$$

2.3.2.5 Peak Signal to Noise Ratio (PSNR)

Peak Signal to Noise Ratio (PSNR) is commonly used to measure the quality of an original image and reconstructed image. PSNR is calculated using the Mean Squared Error (MSE) by;

$$MSE = \frac{1}{MN} \sum_{x=0}^{M=1} \sum_{y=0}^{N=1} \left(I_1(x, y) - I_2(x, y) \right)^2, \tag{9}$$

$$PSNR = 10 \log_{10} \left(\frac{255^2}{MSE} \right), \tag{10}$$

where I_1 and I_2 are the two images, M and N are the row and column number of the images.

2.3.2.6 Structural Similarity (SSIM)

Wang et al. [35] proposed an alternative complementary framework for quality assessment based on the degradation of structural information. To explore the structural information in an image, the luminance and contrast effects are removed from the image. Finally, luminance comparison, contrast comparison and the structure comparison are combined to obtain similarity measure between images. Summary of the structural similarity approach is shown in Figure 8.
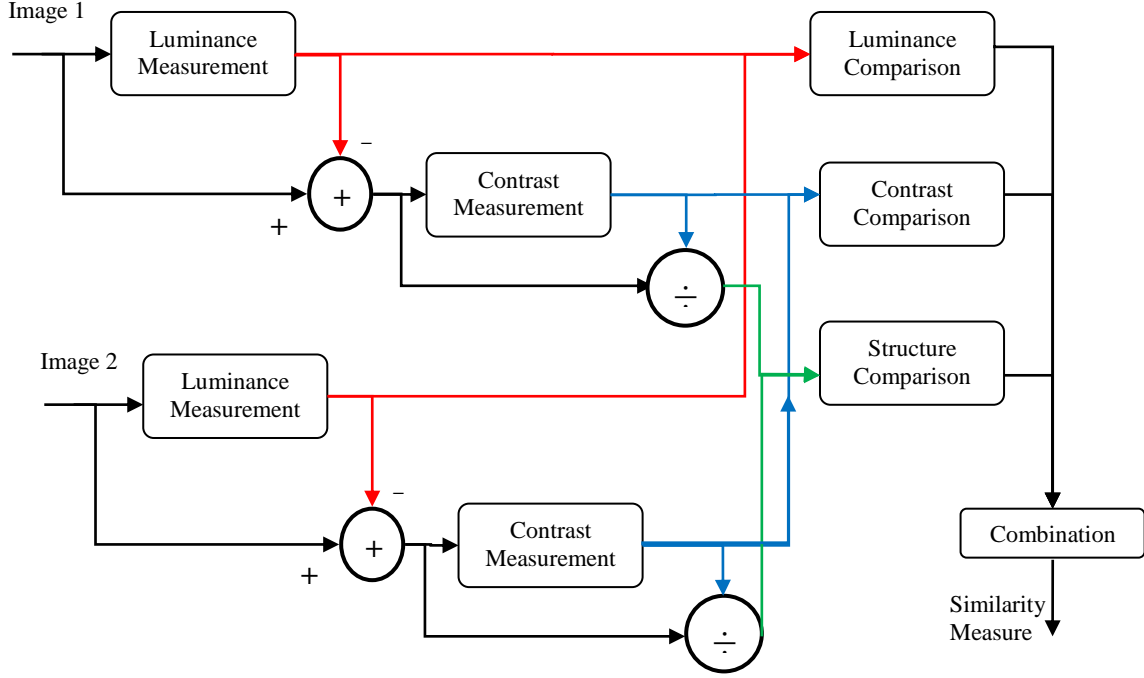

Figure 8 Diagram of structural similarity measurement system

Wang et al. [35] define the structural information in an image that represent the structure of objects in the scene, independent of the average luminance and contrast. They separate the task of similarity measurement into three comparisons: luminance, contrast and structure.

Luminance of each image is calculated as the mean intensity;

$$\mu_{I_1} = \frac{1}{N}\sum_{i=1}^{N} x_{iI_1} \, , \tag{11}$$

where N is the image size. The luminance comparison function $l(I_1, I_2)$ is then a function of μ_{I_1} and μ_{I_2} as

$$l(I_1, I_2) = \frac{2\mu_{I_1}\mu_{I_2} + C_1}{\mu_{I_1}^2 + \mu_{I_2}^2 + C_1}, \tag{12}$$

where the constant C_1 is included to avoid instability. Secondly, Wang et al. [47] use the standard deviation as an estimate of the signal contrast. Standard deviation for a signal is calculated as;

$$\sigma_{I_1} = \left(\frac{1}{N}\sum_{i=1}^{N}\left(x_{I_1} - \mu_{I_1}\right)^2\right)^{\frac{1}{2}}. \tag{13}$$

The contrast comparison $c(I_1, I_2)$ is then a function of σ_{I_1} and σ_{I_2} as

$$c(I_1, I_2) = \frac{2\sigma_{I_1}\sigma_{yI_2} + C_2}{\sigma_{I_1}^2 + \sigma_{I_2}^2 + C_2}, \tag{14}$$

where the constant C_2 is also included to avoid instability.

Third, the structure comparison $s(I_1, I_2)$ is calculated by normalized signals $(I_1 - \mu_{I_1})/\sigma_{I_1}$ and $(I_2 - \mu_{I_2})/\sigma_{I_2}$. The correlation between these two is the measure to quantify the structural similarity. They stated that the correlation between $(I_1 - \mu_{I_1})/\sigma_{I_1}$ and $(I_2 - \mu_{I_2})/\sigma_{I_2}$ is equivalent to the correlation between I_1 and I_2. Thus, the structure comparison is defined as;

$$s(I_1, I_2) = \frac{\sigma_{I_1 I_2} + C_3}{\sigma_{I_1} \sigma_{I_2} + C_3}, \tag{15}$$

where C_3 is added to avoid instability as in luminance and contrast measurements and $\sigma_{I_1 I_2}$ can be estimated as

$$\sigma_{I_1 I_2} = \frac{1}{N} \sum_{i=1}^{N} (I_{1i} - \mu_{I_1})(I_{2i} - \mu_{I_2}). \tag{16}$$

Finally, the three comparisons metrics defined in equations 4.11, 4.13, and 4.14 are combined as;

$$\mathrm{SSIM}(I_1, I_2) = [l(I_1, I_2)]^{\alpha} [c(I_1, I_2)]^{\beta} [s(I_1, I_2)]^{\gamma}, \tag{17}$$

where $\alpha > 0$, $\beta > 0$ and $\gamma > 0$ are parameters used to adjust relative importance of the methods. In this thesis α, β and γ values are all set to 1.

In this article, $c(I_1, I_2)$ is named as SSIM CNTRST, $s(I_1, I_2)$ is SSIM STR, $l(I_1, I_2)$ is SSIM LUM and $SSIM(I_1, I_2)$ is SSIM.

3. EXPERIMENTAL EVALUATION

3.1 Testing Environment

As shown in Figure 9 (a), an object having a characteristic pattern was designed. On the floor, 22 locations were marked in 90 cm intervals. Ground truth object location was measured for one location and the other locations were calculated by using the measured distance and the distance among marks. Images were taken from the tower shown in Figure 9 (b).
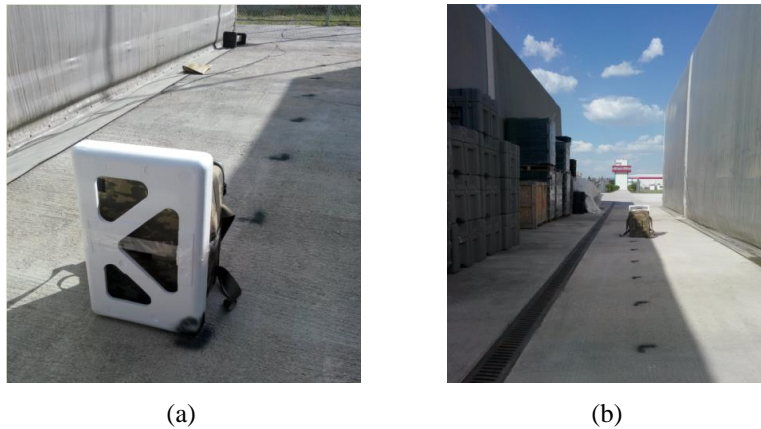

(a)   (b)

Figure 9 Test object and the observation tower

To analyze the performances of comparison methods, artificial blurred reference images are created. Observed images are compared with the reference images with different blur levels. Results of the comparisons are shown in Figure 11. First reference image 1 (image (a) in Figure 10 and sample 1 in Figure 11) is the most blurred reference image and the last image (image (f) in Figure 10 and sample 11 in Figure 11) is the real reference image.

For the first a few sample, reference images are blurred and it is expected that the methods should get lower rates for the first few samples and get higher results for the last samples. However, PwC, HC, MI and PSNR methods do not behave in such a characteristic. Comparison results of all this methods have local maxima at 4th sample and decrease after this sample. Since IB method is not based on the comparison with reference image, this analysis is not applicable for IB method. Performances of the methods are summarized in Table 1.

(a)   (b)   (c)

(d)   (e)   (f)

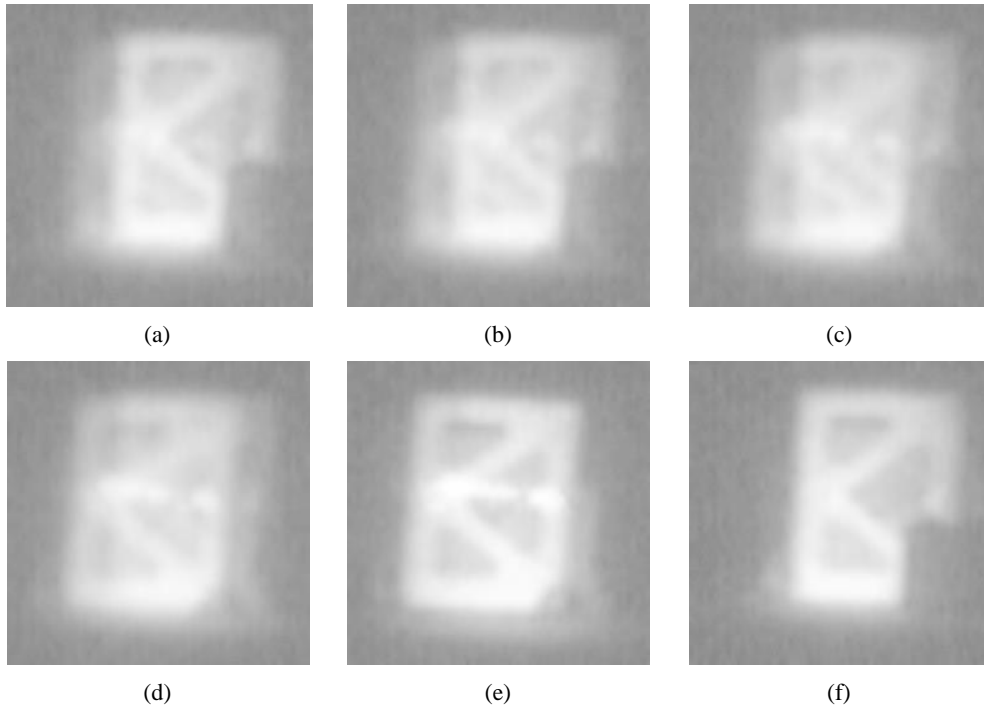Figure 10 Changes in reference images. Object moves and partial occlusion occurs. (a) is the initial reference image, (b)-(e) are the reference images updated at each tracking iteration and (f) is the final reference image. For illustration purposes, dark pixels enhancement is applied by log transform.
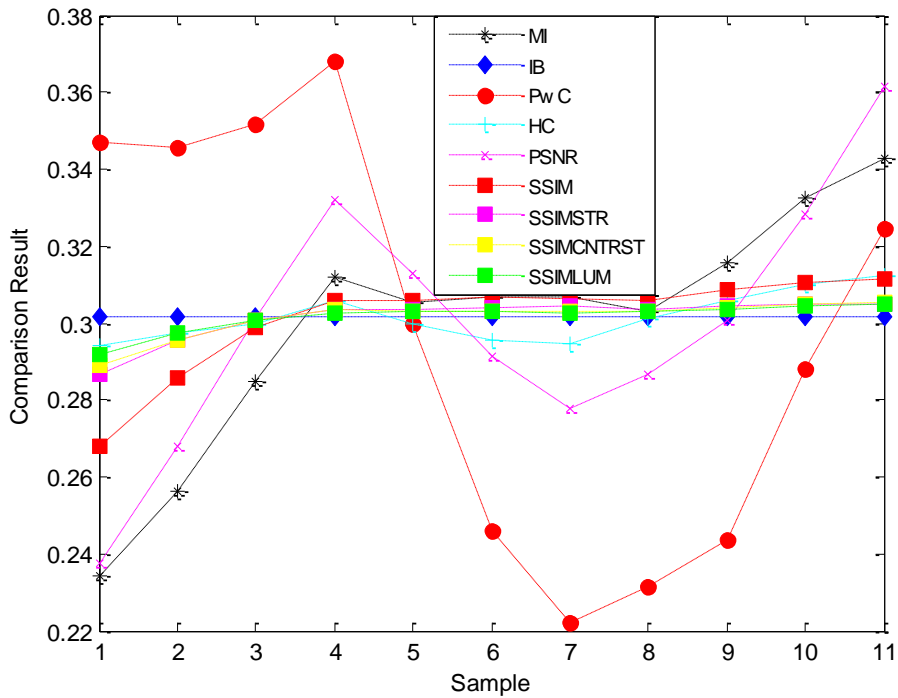

Figure 11 Comparison of the updated reference image and the selected object for each updated reference image

Table 1 Strong and weak sides of methods under different conditions

Method	Blurred Reference Image
HC	POOR
PwC	POOR
IB	N/A
MI	POOR
PSNR	POOR
SSIM	GOOD
SSIM STR	GOOD
SSIM CNTRST	GOOD
SSIM LUM	GOOD

3.2 Test Scenarios

To evaluate the performances of the compared methods, three test images shown in Figure 12 are selected. Standing Man is at 222, Sitting Man is at 204 and the Antenna is at 315 meters distances. Five different data sets are collected with specified three objects. First data set is collected with Standing Man, second set is with Sitting Man and the others are collected with an Antenna. Reflectivities of the all objects are unknown and focus of the laser illuminator is arranged to get desired images. Whole dataset was collected on a summer night with clear weather.
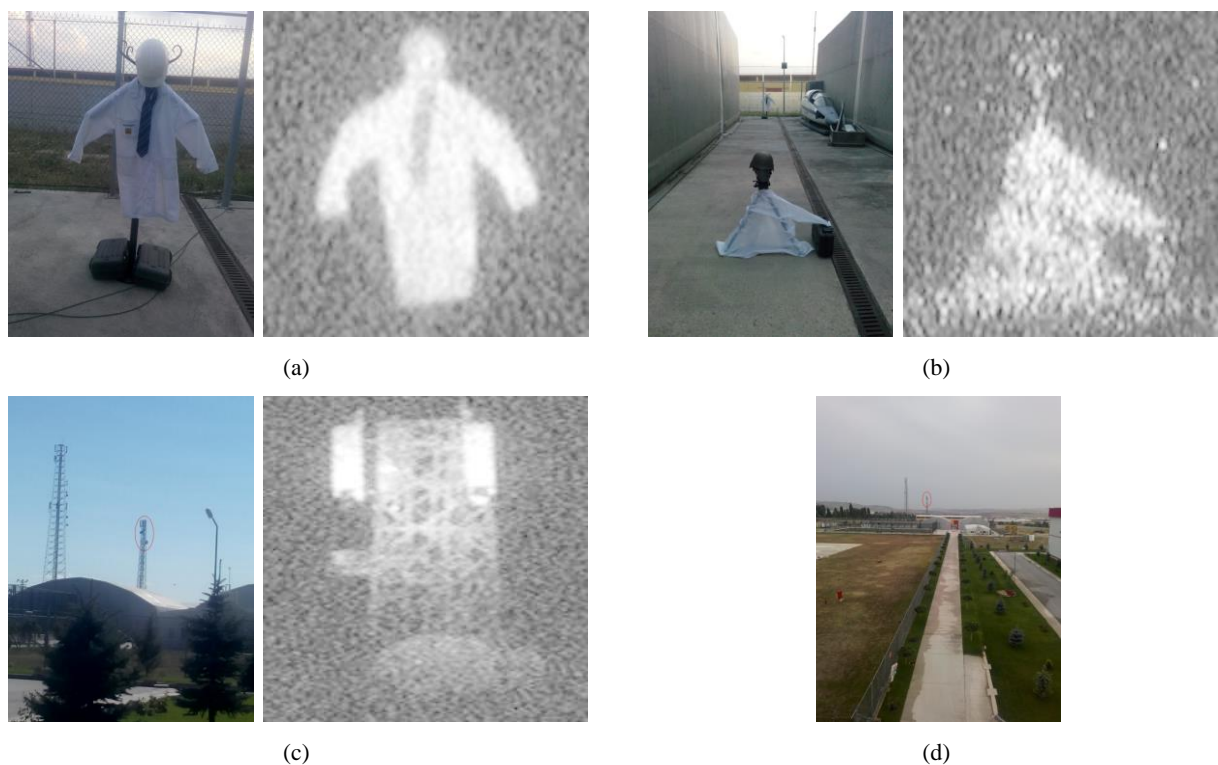

(a)

(b)

(c)

(d)

Figure 12 Objects used in experimental evaluation of compared methods. (a) "Standing Man", (b) "Sitting Man" and (c) "Antenna". (d) the observation tower from where the images of all three objects taken.

3.2.1 Test Scenario 1 (Standing Man)

The object shown in Figure 12 (a) is located around 222 meters distance from observation tower. 19x40 set of images are collected where the object is located 19 different locations. For 19 different object locations, calculated locations and the error values are shown in Figure 13. As shown from the figures, if the object moves more than 1 meter from previous location, errors of the algorithms start to increase. For measuring the performances of the algorithms, locations between -1000 mm and 1000 mm are used.
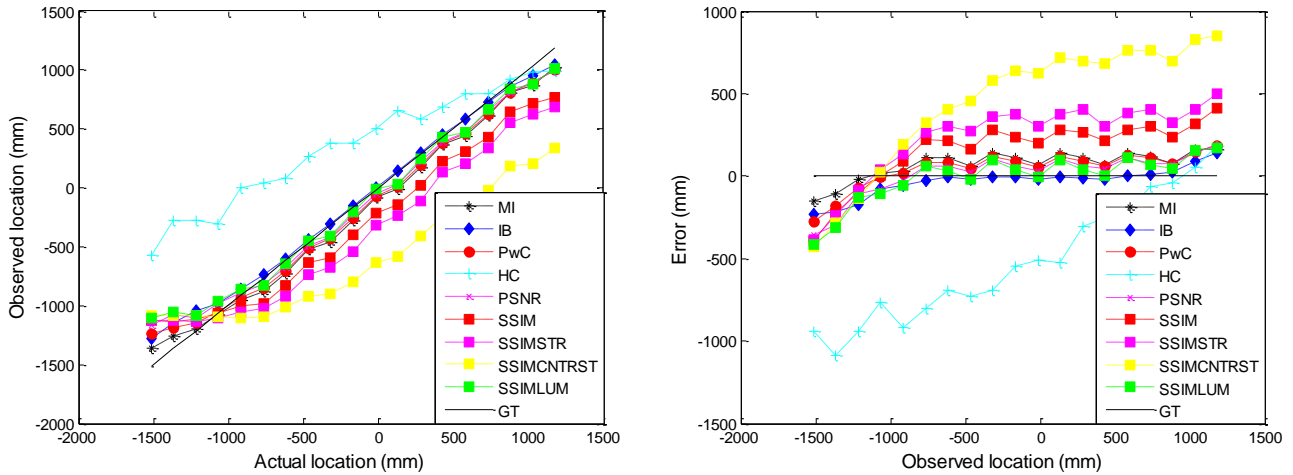

Figure 13 Observed locations (top) and the error values (bottom) for all methods for Standing Man Scenario. Black line is the ground-truth line.

3.2.2 Test Scenario 2 (Sitting Man)

The object shown in Figure 12 (b) is located at around 204 meters from the observation tower. 19x40 set of images are collected where the object is located at 19 different locations. Performances of the methods for both Standing Man and Sitting Man scenarios are shown in Table 2.

Table 2 Error Mean and STD values for all methods for Standing Man and Sitting Man Scenarios. Object is located 15 locations between -1000 mm and 1000 mm. Bold is used to highlight the best result.

Method	Standing Man			Sitting Man		
	Error Mean (mm)	Error STD (mm)	RMS Error (mm)	Error Mean (mm)	Error STD (mm)	RMS Error (mm)
HC	483.6	512.2	704.1	44.5	285.4	288.5
PwC	-82.2	251.5	264.4	143.7	243.4	282.4
IB	11.1	256.1	256.1	28.9	226.2	**227.8**
MI	-99.3	225.4	**246.1**	101.2	218.6	240.7
PSNR	-59.4	258.8	265.3	149.8	261.5	301.1
SSIM	-228.9	276.5	358.7	486.4	911.3	1032.2
SSIM STR	-322.4	281.3	427.7	-104.2	1544.1	1546.2
SSIM CNTRST	-579.4	368.5	686.4	326.3	1038.7	1087.8
SSIM LUM	-39.5	269.5	272.2	103.7	271.7	290.6

3.2.3 Test Scenario 3 (Antenna-3ns StepSize)

The object shown in Figure 12 (c) locates around 315 meters distance from observation tower. 9x40 set of images are collected where the previous location of the object is set to 9 different locations.

3.2.4 Test Scenario 4 (Antenna-2ns StepSize)

The object used in Test Scenario 3 is used for this scenario. The only difference was the step size is set to 2ns. 9x40 set of images are collected where the object is located at 9 different locations.

3.2.5 Test Scenario 5 (Antenna-2ns StepSize Zoom Out)

The object used in Test Scenario 3 and 4 is used for this scenario. The only difference with Test scenario 4 was the lens of the camera is zoomed out. 9x40 set of images are collected where the object is located at 9 different locations.

Table 3 Error Mean and STD values for all methods for Three Antenna Scenarios. Object locations between -900 mm and 900 mm are used. Bold is used to highlight the best result.

Method	Antenna-3ns StepSize			Antenna-2ns StepSize			Antenna- 2ns StepSize Zoom Out		
	Error Mean (mm)	Error STD (mm)	RMS Error (mm)	Error Mean (mm)	Error STD (mm)	RMS Error (mm)	Error Mean (mm)	Error STD (mm)	RMS Error (mm)
HC	215.0	339.6	401.2	238.5	355.2	427.3	271.2	406.7	488.2
PwC	17.2	278.0	277.9	-134.8	306.2	334.0	55.1	329.3	333.3
IB	-131.2	211.3	**248.3**	46.8	310.1	313.1	-62.1	349.8	354.7
MI	60.9	271.3	277.4	-107.6	304.3	322.2	-49.0	323.3	326.4
PSNR	9.0	268.4	267.9	-152.0	313.1	347.6	40.2	323.4	**325.4**
SSIM	136.7	285.4	315.8	-132.6	313.9	340.3	98.1	349.0	362.0
SSIM STR	167.5	304.2	346.6	-89.8	280.4	**294.0**	123.0	339.7	360.7
SSIM CNTRST	405.9	375.7	552.4	-386.9	443.0	587.6	286.3	467.3	547.3
SSIM LUM	43.7	312.7	315.0	-82.0	311.6	321.7	-19.3	350.0	349.9

3.3 Performance Analysis of Test Scenarios

For test setup (5 nanosecond camera gate time and measured laser pulse), illumination function is the convolution of the camera gate time and the laser pulse. Since the system can get images from FWHM/2 cm depth safely, error values between -FWHM/4 cm and FWHM/4 cm can be tolerated. FWHM value for the Imaging Function is 13.48 ns which corresponds 202.2cm. In result, if the error of the range estimation is between -50.55 cm and 50.55 cm, it is assumed as a successful estimation. Success rates of all methods for all scenarios are shown in Table 4.

Table 4 Success rates for all the methods and all the test scenarios

Method	Success Rate (%)					
	Test Scenario 1 Standing Man	Test Scenario 2 Sitting Man	Test Scenario 3	Test Scenario 4	Test Scenario 5	Blurred Reference Image
HC	49.0	92.0	78.7	75.6	69.0	POOR
PwC	94.4	92.8	93.0	86.9	87.0	POOR
IB	95.1	97.3	96.0	89.3	84.5	N/A
MI	96.1	96.5	93.1	88.3	87.8	POOR
PSNR	94.3	90.7	94.0	85.3	87.9	POOR
SSIM	83.8	37.0	89.0	86.2	83.7	GOOD
SSIM STR	74.1	25.6	85.3	91.4	83.8	GOOD
SSIM CNTRST	41.9	35.7	59.7	58.4	63.5	GOOD
SSIM LUM	93.6	91.8	89.1	88.3	85.1	GOOD

3.4 Discussions on Test Results

Main difference between Standing Man and Sitting Man scenarios is the noise levels. It is observed that SSIM CTRST and SSIM STR methods have drawbacks in noisy images. The reason for the SSIM CTRST is observed as the difference noise characteristics of reference image and observed image. Since the reference image is somehow the combination of the previous observed images, it has less noise which affects the contrast characteristic directly.

Test Scenario 1 (Standing Man) is analyzed with different step sizes to understand the effect of the step size on the system performance. For 2 ns step size, 11 images around the object are collected with 2 ns delay between two images. As a result, totally 20 ns depth is searched to find the location of the object. 3 and 4 ns step sizes which means 30 and 40 ns search depth are also investigated. Comparisons are done for only proposed SSIM LUM method.

Success rates for all step sizes are shown in Table 5. It is observed that step size = 3 ns results in best success ratio. It can be concluded that 30 ns search area and 3 ns resolution is a good set of parameters for our setup.

Table 5 Success rates for Standing Man Scenario for 2, 3, 4 ns step sizes

Method	Success Rate (%)		
	Step size = 2 ns	Step size = 3 ns	Step size = 4ns
SSIM LUM	87.3	93.6	89.5

Difference between the Test Scenario 4 and Test Scenario 5 is the optical zoom levels which results on the different noise levels between two images. Although small amount of performance degradation occurs at zoomed out image, there is no significant failure for any of the compared methods.

4. CONCLUSION AND FUTURE WORK

According to the performance results of the methods in Table 4, PwC, IB, MI and SSIM LUM methods have good performance and can all be used for object position estimation. However, only SSIM LUM method has no drawback (IB method has drawbacks for other bright objects) according to Table 4. As a result, SSIM LUM method is proposed for image comparison in range gated object tracking.

For future work, the system can be implemented in real time. By real time implementation, the effect of the accumulated error can be analyzed.

ACKNOWLEDGEMENTS

REFERENCES

[1] Neumann, D. B., "Range Gated Imaging System," U.S. Patent 3.380.358 (1965).

[2] Kerpchar, M., "Range Gated Image System Using Pulsed Illuminators," U.S. Patent 3.689.156 (1972).

[3] Ulich, B.L., Keeler, R. N. and Phlibsen, K., "Lidar System Incorporating Multiple Cameras for Obtaining a Plurality of Subimages," U.S. Patent 4.967.270 (1990).

[4] Ulich, B.L., Keeler, R. N and Phlibsen, K., "Imaging Camera with Adaptive Range Gating," U.S. Patent 5.029.009 (1991).

[5] Bonnier, D. and Larochelle,V., "A range-gated active imaging system for search and rescue, and surveillance operations," Proc. SPIE 2744 Infrared Technology and Applications XXII, (pp. 134-145) (1996).

[6] Repasi, E., Lutzmann, P., Steinvall, O., Elmqvist, M., Göhler, B. and Anstett, G., "Advanced short-wavelength infrared range-gated imaging for ground applications in monostatic and bistatic configurations," Applied Optics. 48, 5956-5969 (2009).

[7] Frecht, A. and Rothe, H., "Comparison of imaging laser radars based on range gating under different weather conditions," Proc. SPIE 3380 Conf. on Laser Radar Technology and Applications III, 292 (1998).

[8] David, O., Kopeika, N.S. and Weizer B., "Range gated active night vision system for automobiles," Applied Optics, 45, 7248-7254 (2006).

[9] Jin, W., Cao, F., Wang, X., Liu, G., Huang, Y., Qi, H., "Range-gated underwater laser imaging system based on intensified gate imaging technology," Proc. SPIE 6621 Photoelectronic Imaging and Detection (2008).

[10] Tan, C., Seet, G., Sluzek, A. and He, D., "A novel application of range-gated underwater laser imaging system (ULIS) in near-target turbid medium," Optics and Lasers in Engineering, 43, 995–1009 (2005).

[11] Driggers, R. G., Vollmerhausen, R. H., Devitt, N., Halford, C. and Barnard, K. J., "Impact of speckle on laser range-gated shortwave infrared imaging system target identification performance," Optical Engineering, 42, 738-746 (2003).

[12] Zhang, S., Zhu, H.O., Wang, L. and Tang S., "Analysis on Detection Range of Laser Active Imaging System," Academic Symposium on Optoelectronics Technology, 236-239 (2010).

[13] Gilles, J., "Restoration algorithms and system performance evaluation for active imagers," Proc. SPIE 6739 Electro-Optical Remote Sensing, Detection, and Photonic Technologies and Their Applications (2007).

[14] Repasi, E., Lutzmann, P., Steinvall, O., Elmqvist, M., Göhler, B. and Anstett, G. "Advanced short-wavelength infrared range-gated imaging for ground applications in monostatic and bistatic configurations," Applied Optics, 48, 5956-5969 (2009).

[15] Espinola, R.L., Jacobs, E.L., Halford, C.E., Vollmerhausen, R. and Tofsted, D.H., "Modeling the target acquisition performance of active imaging systems," Optics Express 15, 3816-3832 (2007).

[16] Busck, J. and Heiselberg, H., "Gated Viewing and High-Accuracy Three-dimensional Laser Radar," Applied Optics, 43, 4705-4710 (2004).

[17] Laurenzis, M., Christnacher, F., Metzger, N., Bacher, E. and Zielenski, I. , "3D range-gated imaging at infrared wavelengths with super-resolution depth mapping," Proc. SPIE 7298, Infrared Technology and Applications XXXV (2009).

[18] Laurenzis ,M. and Bacher, E., "Image coding for three-dimensional range-gated imaging," Applied Optics, 50, 3824-3828 (2011).

[19] Laurenzis ,M. and Bacher, E., Metzger, N. Schertzer, S. and Christnacher , F. , "Coding of range-gates with ambiguous sequences for extended three-dimensional imaging," Proc. SPIE 8542,Electro-Optical Remote Sensing, Photonic Technologies, and Applications VI (2012).

[20] Andersson, P., "Long-range three-dimensional imaging using range-gated laser radar images," Optical Engineering, 45, 034301 (2006).

[21] Monnin, D., Schneider, A. L., Christnacher, F. and Lutz, Y., "A 3D outdoor scene scanner based on a night vision range gated active imaging system," 3D Data Processing, Visualization, and Transmission, Third International Symposium, 938-945 (2006).

[22] Steinvall, O., Andersson, P., Elmqvist, M. and Tulldahl, M., "Overview of range gated imaging at FOI," Proc. SPIE 6542, Infrared Technology and Applications XXXIII, 654216 (2007).

[23] Göhler, B., Lutzmann, P., "Range accuracy of a gated-viewing system as a function of the number of averaged images," Proc. SPIE 8542, Electro-Optical Remote Sensing, Photonic Technologies, and Applications VI, 854205 (2012).

[24] Yilmaz, A. Javed, O. and Shah, M., "Object tracking: A survey," ACM Computing Survey, 38, 4, 13 (2006)

[25] Kristan, M., Pers, J., Kovacic, S. and Leonardis, A., "A localmotion-based probabilistic model for visual tracking," Pattern Recognition, 1, 4 (2009).

[26] Kodama, T., Yamaguchi, T. and Harada, H., " A method of object tracking based on particle filter and optical flow to avoid degeneration problem," SICE Annual Conference, 1529-1533 (2010).

[27] Tung, T. and Matsuyama, T., "Human motion tracking using a color-based particle filter driven by optical flow," ECCV workshop on Machine Learning for Vision-based Motion Analysis ECCV'08 (2008).

[28] Beyan, C. and Temizel, A., "A Multimodal Approach for Individual Tracking of People and Their Belongings," Imaging Science Journal vol. 63, no. 4, pp. 192-202, doi:10.1179/1743131X14Y.0000000101, (2015).

[29] Spies, H., Jähne, B. and Barron, J., " Range Flow Estimation," Computer Vision and Image Understanding, 85, 209-231 (2002).

[30] Barron, J.L. and Spies, H., "The Fusion of Image and Range Flow," Lecture Notes in Computer Science, 2032, 171-189 (2001).

[31] Wren, C., Azarbayejani A. and Pentland, A., " Pfinder: Real-time tracking of the human body," IEEE Trans. Patt. Analy. Mach. Intell. 19, 7, 780–785 (1997).

[32] Beyan, C. and Temizel, A., "Adaptive Mean-Shift for Automated Multi Object Tracking," IET Computer Vision, 6, 1, 1-12, doi:10.1049/iet-cvi.2011.0054, (2012).

[33] Beyan, C. and Temizel, A., "Mean-shift tracking for surveillance applications using thermal and visible band data fusion", Proc. SPIE 8020, Airborne Intelligence, Surveillance, Reconnaissance (ISR) Systems and Applications VIII, 802010 (2011);

[34] Russakoff, D. B., Tomasi, C., Rohlfing, T. and Maurer Jr, C. R. "Image similarity using mutual information of regions," Computer Vision-ECCV, 596-607 (2004).

[35] Wang, Z., Bovik, A.C., Sheikh, H. R. and Simoncelli, E. P. "Image Quality Assessment: From Error Visibility to Structural Similarity," IEEE Transactions on Image Processing, vol. 13, no. 4, pp. 600-612, (2004).